In-Situ Thermal Battery Discharge using NiS$_2$ as a Cathode Material

Julia L. Payne,*[a] Julia D. Percival,[b] Kyriakos Giagloglou,[a] Christina J. Crouch,[a, b] George M. Carins,[a] Ronald I. Smith,[c] Robert Comrie,[d] Richard K. B. Gover,[b] and John T. S. Irvine*[a]

NiS$_2$ is a cathode material found in primary batteries which operate at high temperature. Herein we report the *in situ* battery discharge study of a thermal battery cell which uses NiS$_2$ as a cathode, using simultaneous collection of powder neutron diffraction data and electrochemical data. Five different regions were observed upon battery discharge and the evolution of nickel sulfide phases has been studied. Four different nickel-containing phases are observed during dis-charge (NiS$_2$, NiS, Ni$_3$S$_2$ and Ni). A new discharge mechanism has been proposed which does not include Ni$_7$S$_6$. Multiphase quantitative Rietveld refinement has allowed the percentages of the phases to be monitored during discharge. High intensity synchrotron powder X-ray diffraction has been used to study the resulting phases present in the cathode after battery discharge.

1. Introduction

Thermal batteries are a well-known primary battery technology which finds use in applications such as emergency power supplies in aircraft.[1] These applications require a constant power to be drawn from the battery over a length of time and as a result, thermal batteries which undergo conversion reactions rather than intercalation discharge reactions are preferred.

Typically a thermal battery consists of four components: the anode, the electrolyte, a separator and the cathode. The anodes are often a binary or ternary lithium alloy, such as Li$_x$Si$_y$, Li$_x$Al$_y$ or Li$_x$Sn$_y$, but the Li$_{13}$Si$_4$ anode has received a significant amount of attention due to its moisture insensitivity, high lithium mobility and its higher voltage in comparison to other anode materi-als.[2,3] The proposed discharge mechanism in Li$_{13}$Si$_4$ is thought to be Li$_{13}$Si$_4$→Li$_7$Si$_3$→Li$_{12}$Si$_7$, with the final products in batteries which utilise a sulfur based cathode being Li$_2$S and Si.[3,4]

The electrolyte consists of a molten salt, which is solid at room temperature and therefore does not exhibit any ionic conductivity.[5] Typically a pyrotechnic source is used to heat the battery above the melting point of the electrolyte. As a result, the electrolyte becomes molten, and the conductivity of the electrolyte increases. The LiCl-KCl eutectic is one of the favoured molten salt electrolytes due to properties such as the melting point (compatible with respect to thermal decomposi-tion of the anode and cathode), the high ionic conductivity and the low solubility of the discharge products in the electrolyte.[5]

Metal sulfides, metal halides and metal oxides have all been explored as potential cathode materials.[6] These cathode materials must satisfy a range of criteria, such as a high electronic conductivity, thermal stability, insolubility in the molten salt electrolyte, insolubility of discharge products in the molten salt and the inability to be oxidised by the electro-lyte.[6,7] Some of the most widely studied cathode compositions are transition metal sulfides. The NiS$_2$, FeS$_2$ and CoS$_2$ cathodes have been widely studied, but the suggested discharge mechanisms are different, depending on the transition metal used in the cathode.[6,7] Existing studies have involved carrying out the battery discharge and then stopping the measurement at a particular voltage, and then collecting diffraction data (along with other chemical measurements) at room temper-ature. Alternatively electrochemical measurements may be carried out at device operating temperatures, but are unable to probe the crystalline phases present. This can lead to difficulties in understanding the high temperature structure, due to differences in crystal structure or phase stability between device operating temperature and room temperature. Therefore, despite being used for many years, little is known about how the crystalline phases in the battery evolve at high temper-ature.

[a] Dr. J. L. Payne, K. Giagloglou, C. J. Crouch, Dr. G. M. Carins, Prof. J. T. S. Irvine
School of Chemistry
University of St Andrews
North Haugh
St Andrews Fife KY16 9ST (UK)
E-mail: jlp8@st-andrews.ac.uk
jtsi@st-andrews.ac.uk
[b] Dr. J. D. Percival, C. J. Crouch, Dr. R. K. B. Gover
AWE
Aldermaston
Reading RG7 4PR (UK)
[c] Dr. R. I. Smith
ISIS Facility
STFC Rutherford Appleton Laboratory
Harwell Campus
Didcot OX11 0QX (UK)
[d] Dr. R. Comrie
MSB Ltd
Hagmill Road
East Shawhead, Coatbridge ML5 4UZ (UK)

The Ni–S phase diagram was extensively studied by Kullerud and Yund and it was later revisited by Lin *et al.*[8,9] Several Ni–S phases have been reported, which include NiS, $Ni_{1-x}S$, NiS_2, Ni_3S_2, $Ni_{3\pm x}S_2$, Ni_3S_4 and Ni_7S_6 and a number of these phases exhibit polymorphism.[8] At 520 °C, NiS_2, NiS, $Ni_{1-x}S$, Ni_3S_2 and $Ni_{7\pm x}S_6$ are stable. The area of the phase diagram around $Ni_{7\pm x}S_6$ has been found to be quite controversial and Seim *et al.* found that the thermal history of the sample strongly affected the phases that were observed.[10] This was partly attributed to the high degree of Ni disorder in Ni_7S_6 which was first reported by Fleet and it has been suggested that quenching can result in different Ni distributions.[10, 11] Work on this region of the phase diagram by Seim *et al.* suggested that there are four metastable phases in this compositional region.[10] Recently, Withers *et al.* have revisited this region of the Ni–S phase diagram and have found the presence of an incommensurate phase and also an $I1a1$ phase which is a superstructure of the Ni_7S_6 $Bmmb$ cell, with no evidence of any other polymorphs.[12] Despite the detailed study of this region in the phase diagram, by a range of techniques, the detailed crystallographic analysis (especially in terms of atomic coordinates, site occupancies *etc.*) of these phases is still lacking.[10]

NiS_2 adopts the pyrite structure (space group Pa-3) and consists of a face-centred array of Ni atoms, which sit at the centre of slightly distorted corner sharing NiS_6 octahedra. At temperatures above 379 °C NiS adopts the NiAs structure (space group $P6_3/mmc$), with sulfur atoms sitting at the centre of trigonal prisms. Ni_3S_2 adopts the Heazlewoodite structure (space group $R32$) and can be viewed as a network of corner sharing, sulfur centred SNi_6 trigonal bipyramids, with different Ni–Ni distances for the two triangular Ni_3 faces of the trigonal pyramids. The NiS_2 (pyrite), NiS (NiAs structure) and Ni_3S_2 (heazlewoodite) structures are shown in Figure 1.
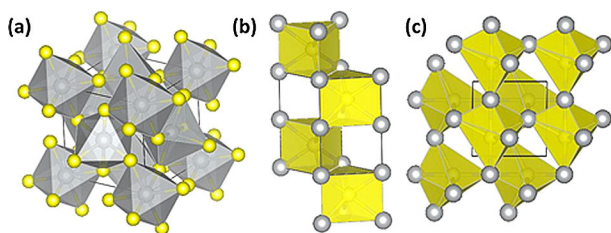

Figure 1. Structures of (a) NiS_2 with the pyrite structure (b) NiS with the NiAs structure and (c) Ni_3S_2 with the Heazlewoodite structure. Nickel is shown in grey and sulfur in yellow, with the polyhedra shaded according to the atom at the centre of the polyhedron.

DFT studies have simulated the cell discharge of secondary batteries at room temperature which utilise FeS_2 or NiS_2 as the cathode.[13] Here, they proposed that the final discharge products are Li_2S and either Fe or Ni, with Li_2FeS_2 or Li_2NiS_2 being intermediate phases in the discharge.[13] However, the formation of Li_2NiS_2 has not been reported experimentally. Interestingly it was found that the enthalpies of formation of different nickel sulfides are very close but have different

theoretical capacities.[13] Therefore, cells which use NiS_2 as a cathode in a secondary cell, display poorer cycling capability.

In-situ powder neutron diffraction has been used as a tool to correlate the structure with the electrochemical properties in batteries since the 1990's and an early example includes the characterisation of the electrochemical extraction of lithium from $LiMn_2O_4$.[14] Since then, a range of cell designs and materials have been explored in order to correlate the structure with the electrochemical properties by carrying out *in-situ* powder neutron diffraction experiments.[15] Existing studies have focused on room temperature, rechargeable batteries, and to date, to the best of our knowledge, no *in-situ* powder neutron diffraction studies of high temperature thermal batteries have been reported. Powder neutron diffraction is particularly suitable for studying lithium containing compounds, due to lithium's much higher scattering power relative to the other "heavy" atoms in the battery (e.g. Ni, S) with neutrons than with X-rays. The use of neutron diffraction in this study is particularly important, given the sensitivity to lithium, especially given the differences in the discharge mechanisms between the FeS_2 cathode, which reportedly forms lithiated compounds upon discharge and the NiS_2 cathode which reportedly does not form lithiated compounds upon discharge.[6, 7, 16] The aim of this work was to probe the discharge mechanism of a thermal battery employing a NiS_2 cathode using *in-situ* powder neutron diffraction.

2. Results and Discussion

Before carrying out the *in-situ* neutron diffraction experiment, battery discharge was carried out on the NiS_2 battery galvanostatically at 520 °C, in order to identify the voltage plateaux, so that the in situ neutron diffraction experiment could be carried out potentiostatically. The battery discharge profile is shown in Figure 2. Three plateaux are observed at voltages of 1.71 V, 1.44 V and 1.24 V. This is comparable to the values of 1.740, 1.591, 1.545 and 1.358 V reported by Preto *et al.* at 400 °C using a Li–Al anode. Plateaux were also reported at approximately 1.75 V and 1.25 V by Guidotti, with the ~1.75–1.25 V regions showing several inflections in the data in a test carried out at 500 °C with a Li–Si anode.[6, 16] In our experiment, the anode is not in excess with respect to the cathode, so therefore the changes in voltage due to lithium removal from $Li_{13}Si_4$ must also be considered. This has been studied previously by Wen and Huggins, who reported that at 415 °C the $Li_{13}Si_4$ to Li_7Si_3 transition occurs at 158 mV (w.r.t. Li), whilst the Li_7Si_3 to $Li_{12}Si_7$ transition occurs at 288 mV (w.r.t. Li).[3] This corresponds to a difference of 130 mV when going from the $Li_{13}Si_4/Li_7Si_3$ plateau to the $Li_7Si_3/Li_{12}Si_7$ plateau. The $Li_{13}Si_4/Li_7Si_3$ plateau will give a capacity of 107 mAh in this experiment (based on 0.22 g of anode) Therefore in Figure 2, the ~135 mV drop in voltage close to $x = 1.0$ Li per NiS_2, (which corresponds to an anode capacity of 97 mAh) is due to the transitions occurring in the anode. Below $x = 1.0$ the voltage is relative to the $Li_{13}Si_4 \rightarrow Li_7Si_3$ transition, whilst above $x = 1.0$, the voltage is relative to the $Li_7Si_3 \rightarrow Li_{12}Si_7$ transition. A capacity of
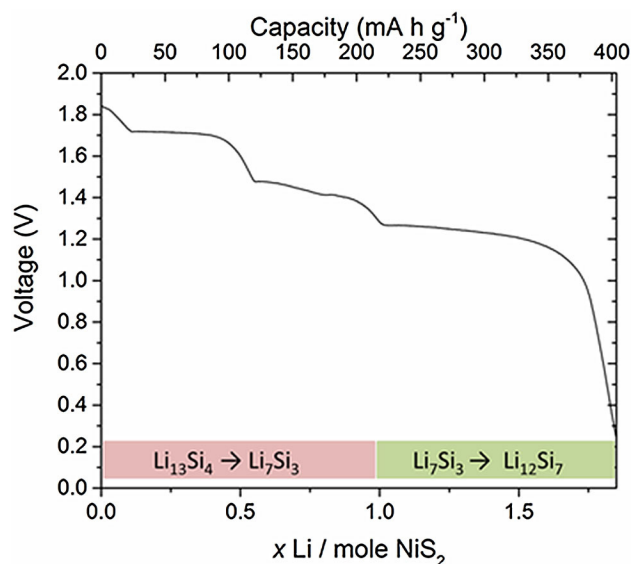
Figure 2. Battery discharge profile for a NiS_2 cell discharged galvanostatically using a current density of 23 mA cm^{-2}. The state of the anode is indicated at the bottom of the figure.
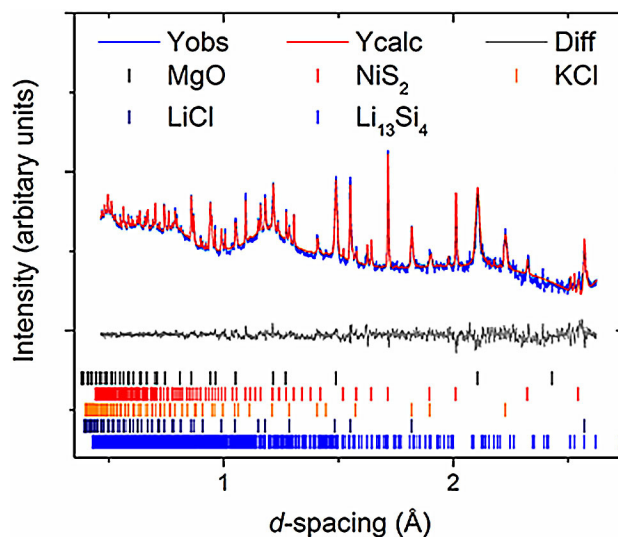

Figure 3. Multiphase Rietveld fit to powder neutron diffraction data collected from the NiS_2 cell before discharge, at room temperature.
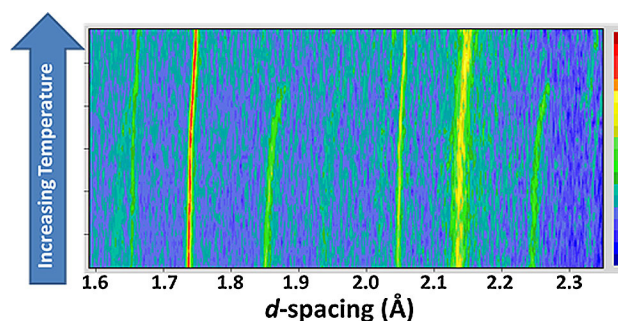

Figure 4. Film plot of diffraction data upon heating (Polaris backscattering detectors). Peaks that disappear upon heating are due to the KCl-LiCl eutectic electrolyte. Note that the y-axis is not a linear function of temperature, but is a function of diffraction dataset.
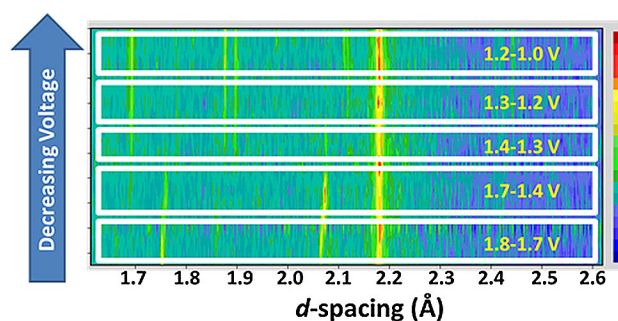

Figure 5. Film plot of powder neutron diffraction data collected during discharge of a thermal battery utilising a NiS_2 cathode (Polaris backscattering detectors). Note that the y-axis is a function of diffraction pattern number and as a result is not a linear function of voltage or time as it includes the data collected at isopotentials.

403 mA h g^{-1} was achieved for this NiS_2 cell which corresponds to an x of 1.85 Li per mole of NiS_2. The value of x per mole of NiS_2 and capacity is lower than reported in the literature, due to slightly less capacity being extracted from the first voltage plateau at 1.71 V.

Powder neutron diffraction data were collected from the battery at room temperature before the *in-situ* discharge experiment (Figure 3). As the KCl-LiCl eutectic is solid at room temperature, the diffraction pattern shows the presence of KCl and LiCl, along with the MgO separator and NiS_2.

At room temperature, NiS_2 can be described using the cubic pyrite structure whilst LiCl, KCl and MgO adopt the rock-salt structure. The anode suffered from preferred orientation/texture effects resulting in a poor fit to the observed intensities from this phase. Consequently, its contribution to the diffraction pattern was modelled using a Le Bail intensity extraction method. Figure 3 shows the Rietveld fit to the neutron powder diffraction data obtained at room temperature.

Batteries employing a NiS_2 cathode and a LiCl-KCl eutectic electrolyte exhibit good electrochemical performance at 520°C, which is sufficiently above the melting point of the eutectic that it will enable a high ionic conductivity and hence this temperature was chosen for the in situ battery discharge. Neutron powder diffraction data were collected on heating the cell from room temperature until 520°C and this is shown in Figure 4. The peaks that disappear (e.g. at d-spacings of 1.85 Å and 2.25 Å) are due to the melting of the LiCl-KCl eutectic. Note that the apparent deviation from linearity in Figure 4 is due to the y- axis being a function of dataset number.

Once the cell had reached 520°C, the cell was discharged. Figure 5 shows a film plot of the neutron powder diffraction data collected during discharge. The cell was discharged potentiostatically, and longer duration, higher quality data sets were collected at isopotentials of 1.8 V, 1.7 V, 1.4 V, 1.3 V, 1.2 V

and 1.0 V. These isopotentials are combined with shorter duration data sets and are shown together in Figure 5 so the y-axis is not a linear function of voltage or time, but diffraction dataset number. Five regions could be observed in the

diffraction patterns, for voltages between 1.8–1.7 V, 1.7–1.4 V, 1.4–1.3 V, 1.3–1.2 V and 1.2–1.0 V. The evolution of the phases will be discussed in more detail below.

Figure 6a-f show the Rietveld fits to the data collected at different isopotentials. The structured background is mainly due to the significant contribution of the amorphous quartz sample container but there will also be a contribution from the molten LiCl-KCl electrolyte. This background was modelled using the Debye equation which is implemented within the diffuse scattering function in GSAS and could be well modelled with seven diffuse scattering parameters based on the Si–O, Si–Si and O–O interatomic distances in quartz. In addition, a further four parameters using the reciprocal linear interpolation function were included in the refinement to account for the
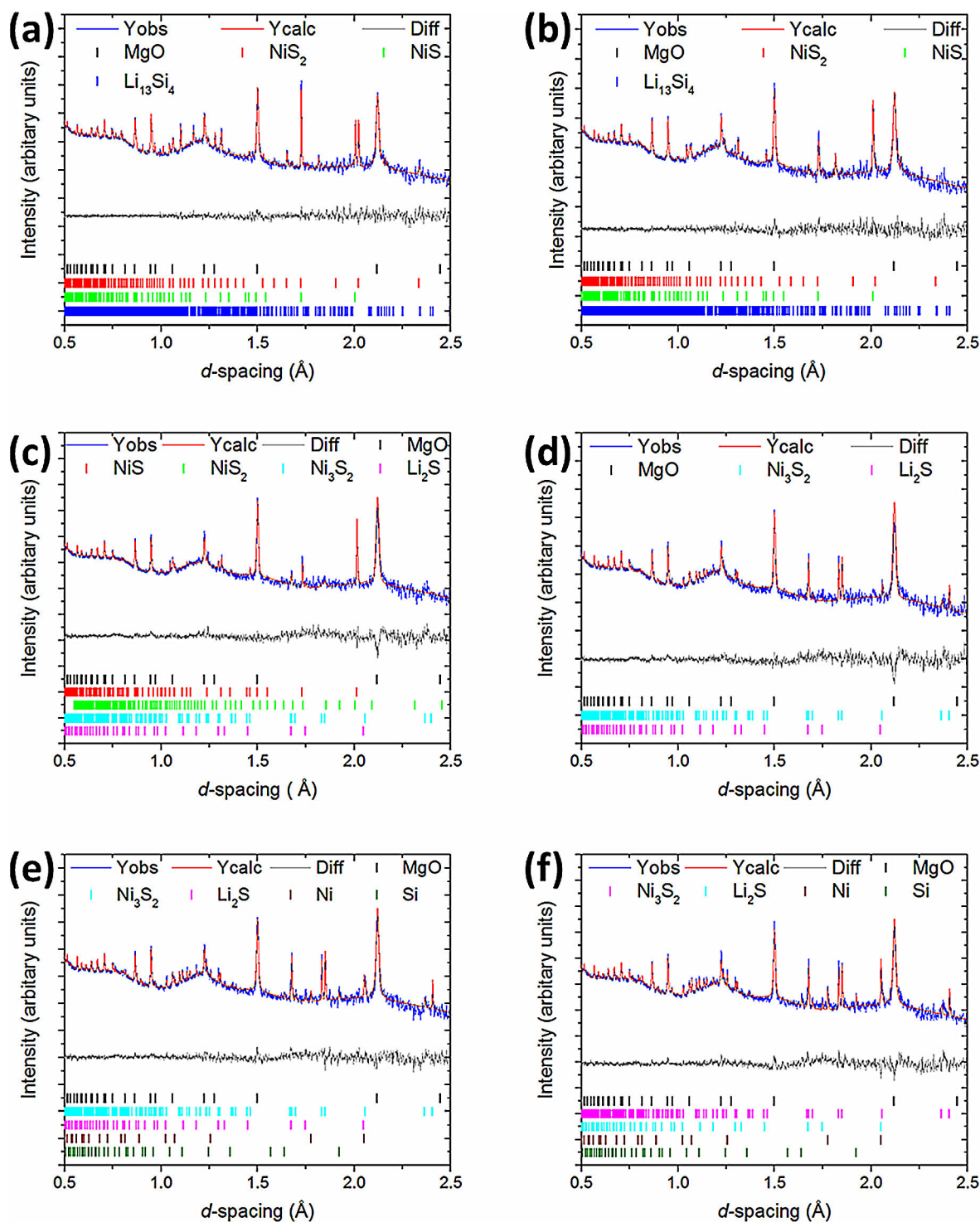

Figure 6. Multiphase Rietveld fits to isopotential data collected at a) 1.8 V, b) 1.7 V, c) 1.4 V, d) 1.3 V, e) 1.2 V and f) 1.0 V.

overall decrease in background over the *d*-spacing range used. The background was fixed in the latter stages of refinement. Cell parameters, scale factors, atomic coordinates (NiS_2 and Ni_3S_2 phases only) and peak widths were refined for each phase present in the refinement. Data were not of sufficient quality to extract reliable thermal parameters. The lower signal to noise ratio in the powder neutron diffraction patterns are due to a relatively thin battery being used which allows more realistic electrochemical performances to be obtained. MgO from the separator is clearly observed in all diffraction patterns. The resulting phase fractions (as weight percent) were extracted from the refinements and have been plotted in Figure 8 with the battery voltage discharge profile and will be discussed in conjunction with the discussion of the refinements below. Unit cell parameters of the battery discharge products at 520 °C are listed in Table 1.

Figure 7. Variation of NiS cell parameter with voltage a) NiS *a* cell parameter and b) NiS *c* cell parameter.

Table 1. Unit cell parameters of crystalline phases at 520 °C

Phase	Unit cell parameters at 520 °C [Å]		
MgO	$a = 4.23730(12)$		
$Li_{13}Si_4$	$a = 7.9337(11)$	$b = 15.157(2)$	$c = 4.4975(6)$
NiS_2	$a = 5.71814(17)$		
NiS	$a = 3.4508(4)$	$c = 5.4072(9)$	
Ni_3S_2	$a = 4.11425(17)$	$\beta = 89.260(6)°$	
Li_2S	$a = 5.7978(6)$		
Ni	$a = 3.5504(2)$		
Si	$a = 5.4373(11)$		

At 1.8 V and 1.7 V, NiS_2 and NiS ($P6_3/mmc$) are both present in the diffraction data (Figure 6a and b). Multiphase Rietveld refinement which incorporated MgO, NiS_2 and NiS structural models failed to model a peak at 1.81 Å. This peak could be fitted using a Le Bail fit, using the cell parameters and space group of $Li_{13}Si_4$, hence this peak was attributed to the anode. It should be pointed out that several structural models have been proposed for $Li_{13}Si_4$, but Rietveld refinements using these models did not adequately fit this peak. As the existing $Li_{13}Si_4$ structural models result from X-ray diffraction studies at low temperature or computational simulations, further structural work is required to gain a detailed study of the $Li_{13}Si_4$ structure at elevated temperatures.[21] During the discharge, the cell parameters of NiS increase, as shown in Figure 7. Possible explanations for this increase in cell parameter could be the incorporation of a small amount of lithium into this phase, given the larger radius of Li^+ (0.76 Å) with respect to Ni^{2+} (0.69 Å) in six fold coordination,[22] or alternatively a gradually evolving degree of non-stoichiometry in the NiS phases, resulting in the presence of $Ni_{1-x}S$ phases. The 1.8–1.7 V voltage range corresponds to the first plateau observed in the discharge profile of NiS_2. This indicates that the first plateau in the discharge profile of the battery can be attributed to the NiS_2 to NiS transformation.

At 1.4 V (Figure 6c), the major phase present is NiS ($P6_3/mmc$) with Li_2S and a very small amount of Ni_3S_2. The peak at 1.81 Å which was attributed to the anode was no longer apparent at this voltage and no peaks from other lithium
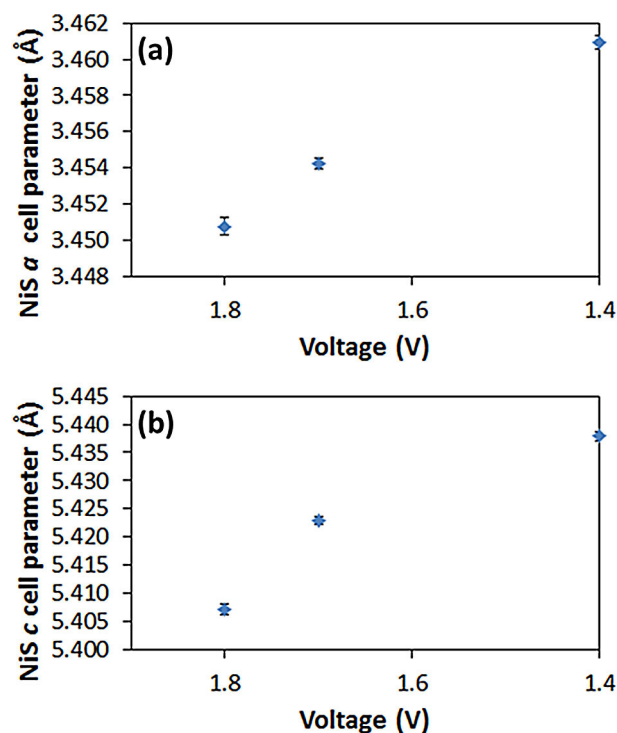
silicides which are expected to form during the discharge were observed. It is likely that there is a loss in crystallinity and amorphisation of $Li_{13}Si_4$ and the related lithium silicides at high temperatures and upon lithium extraction, which is why peaks from lithium silicides are no longer observed in the diffraction pattern during discharge. This is perhaps unsurprising considering the known electrochemically driven amorphisation of Li_xSi_y phases formed during the lithiation of silicon at room temperature reported by Dudney et al.[23]

At 1.3 V (Figure 6d), Ni_3S_2 is observed in the diffraction patterns. This indicates that the NiS to Ni_3S_2 transformation is responsible for the second plateau in the battery discharge profile. At no point is Ni_7S_6 observed in the diffraction patterns during discharge. This is particularly significant as previous studies had reported that Ni_7S_6 was an intermediate phase in the discharge of thermal batteries with NiS_2 cathodes.[16] The lack of Ni_7S_6 in the discharge mechanism could be due to several possibilities such as the metastability of this phase or the use of different anodes and temperatures in the previous studies.

As the discharge proceeds, the final products of the discharge reaction, Ni, Li_2S and Si, gradually appear in the diffraction patterns for the 1.2 V and 1.0 V isopotentials (Figure 6e and f). Lithium sulfide (Li_2S) and silicon from the $Li_{13}Si_4$ anode could be observed clearly in the later stages of the discharge. In the final stages of battery discharge, a slope is observed in the battery discharge profile, from 1.2 V to 1.0 V. This corresponds with the formation of the final discharge reaction products of Ni and Si and their appearance in the diffraction patterns. It is worth noting that in this experiment,

at 1.0 V, the Ni_3S_2 phase had not completely transformed into Ni metal and Li_2S.

The phase fractions extracted from the refinements are shown in Figure 8 along with the battery discharge profile
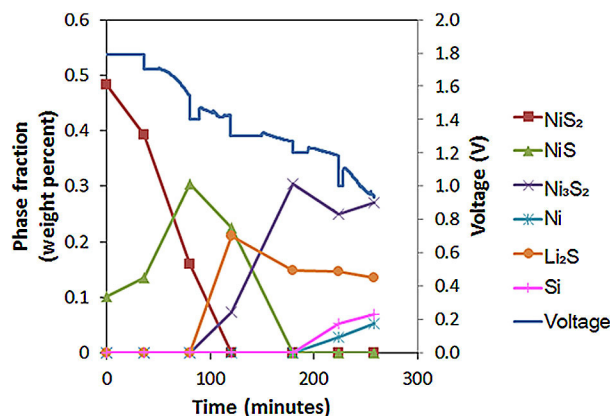

Figure 8. Voltage discharge profile and phase fraction as a function of time. Note that MgO phase fractions have been excluded for clarity.

collected during the diffraction data collection. The phase fraction may also be plotted as a function of voltage, as shown in Figure 9. At $t = 0$ minutes (at $520\,°C$) there is some NiS
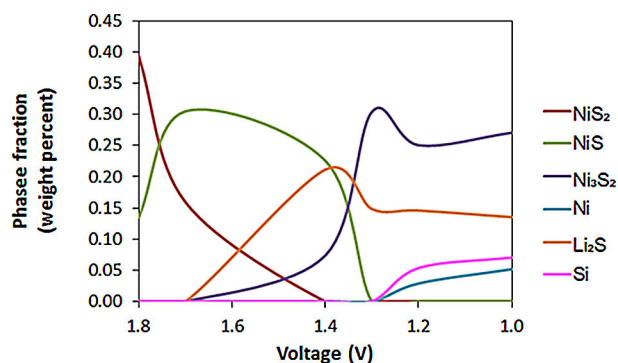

Figure 9. Phase fraction as a function of voltage.

present in the diffraction pattern, which has been attributed to a small degree of self-discharge of the cell once the eutectic melting point had been reached. It should be noted that no NiS was observed in our room temperature neutron diffraction data (see Figure 3). As can be seen from Figure 8, as the amount of NiS_2 decreases, the fraction of NiS increases. This corresponds to the first plateau in the discharge profile. At the end of the first plateau, Li_2S appears in the diffraction pattern. The fraction of NiS decreases as the phase fraction of Ni_3S_2 increases, where it reaches a maximum at 1.3 V (Figure 8). This transformation of NiS to Ni_3S_2 corresponds to the second plateau in the discharge profile (Figure 8). Finally, the last step in the discharge procedure is the formation of Ni and Si and this can be attributed to the slope at the end of the discharge profile (Figure 8). It should be noted that we stopped the discharge at

1.0 V (at a voltage where such batteries would no longer be useful) but the complete conversion of Ni_3S_2 to Ni and Li_2S had not occurred at this point.

Room temperature synchrotron powder X-ray diffraction data was used to confirm the final products of battery discharge. The cathode was scraped from the battery cell after the neutron diffraction experiment and loaded into a quartz capillary in the glovebox to prevent any exposure of the sample to moisture and air. Seven crystalline phases could be observed in the diffraction pattern: Ni_3S_2, Ni, Li_2S, MgO, KCl, LiCl and $LiVS_2$ and the corresponding multiphase Rietveld fit is shown in Figure 10, with corresponding structural parameters being
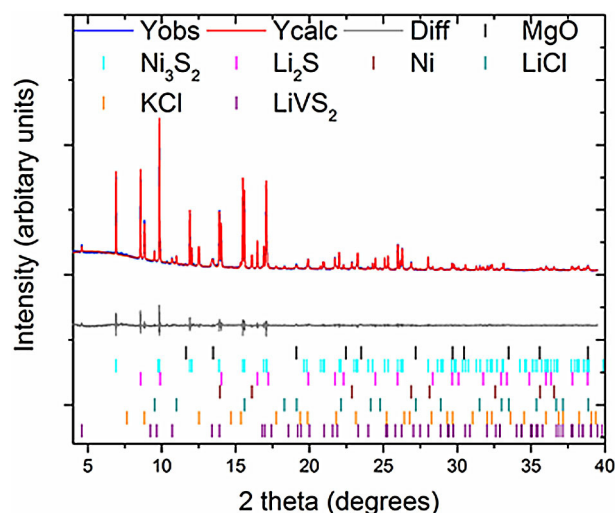

Figure 10. Multiphase Rietveld fit to synchrotron PXRD data collected on cathode material after the in situ neutron diffraction experiment.

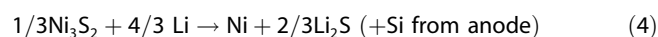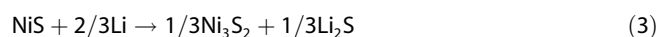| Table 2. Unit cell parameters (at room temperature) of cell discharge products after in situ neutron diffraction experiment.		
Phase	Unit cell parameters at room temperature [Å]	
Ni	$a = 3.52422(7)$	
Ni_3S_2	$a = 4.081969(3)$	$\beta = 89.462(6)°$
Li_2S	$a = 5.72469(9)$	
LiCl	$a = 5.1475(2)$	
MgO	$a = 4.2056(4)$	
KCl	$a = 6.39977(18)$	
$LiVS_2$	$a = 3.3979(4)$	$c = 6.1173(15)$

reported in Table 2. The small amount of $LiVS_2$ observed, which was not observed in the neutron diffraction patterns is probably due to a small reaction of lithium sulfide with the vanadium current collector at the end of the battery discharge. The presence of LiCl and KCl is due to the electrolyte solidifying on cooling along with the difficulty in separating the cathode from the LiCl/KCl/MgO electrolyte/separator pellet at the end of the reaction. Silicon was not observed in this cathode sample,

presumably as the silicon remains on the anode side once formed during battery discharge.

The mechanism for NiS_2 discharge in a thermal battery was first studied by Preto et al. in 1983 using cyclic voltammetry.[16] They outlined the following discharge mechanism at 400 °C using a Li—Al anode, which gave plateaux at 1.740, 1.5951, 1.545 and 1.358 V [Eq. (1)]:[16]

$$NiS_2 \rightarrow NiS + Li_2S \rightarrow Ni_7S_6 + Li_2S \rightarrow Ni_3S_2 + Li_2S \rightarrow Ni + Li_2S \tag{1}$$
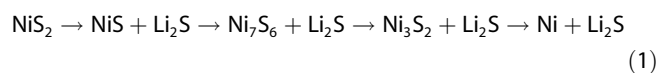
In our experiment, Ni_7S_6 was not observed in the discharge process. We can now write a modified mechanism [Eqs. (2)–(4)] for the NiS_2 discharge at 520 °C using a $Li_{13}Si_4$ anode:

$$NiS_2 + 2Li \rightarrow NiS + Li_2S \tag{2}$$

$$NiS + 2/3Li \rightarrow 1/3Ni_3S_2 + 1/3Li_2S \tag{3}$$

$$1/3Ni_3S_2 + 4/3\,Li \rightarrow Ni + 2/3Li_2S\ (+Si\ from\ anode) \tag{4}$$

At the end of the first and second plateaus, the molar ratios of NiS_2 and Li_2S (plateau one) Ni_3S_2 and Li_2S (plateau two) extracted from Rietveld refinement are in good agreement with the expected 1:1 molar ratios for the reaction. As discussed earlier we did not observe complete transformation of Ni_3S_2 to Ni and Li_2S during this experiment, hence the $Ni:Li_2S$ molar ratios are lower than expected

3. Conclusions

In-situ powder neutron diffraction has been used to probe the structure-property relationships in thermal batteries which utilise NiS_2 as a cathode. This is the first combined diffraction and electrochemical study of a thermal battery and has been carried out at device operating temperature. Changes in lattice parameters for NiS warrant further detailed investigation on bulk single phase samples to understand the structural features and possible Li incorporation which cause the increase in cell parameters. Multiphase Rietveld refinement has provided no evidence for the formation of Ni_7S_6, a phase which was previously thought to participate in the discharge reaction of NiS_2 cathodes. This has enabled us to propose a new discharge mechanism for NiS_2 cathodes. Further studies are required to fully understand the structure and discharge behaviour of the $Li_{13}Si_4$ anode at elevated temperatures.

Experimental Section

$Li_{13}Si_4$ (anode, 0.22 g, 1.1 mmol), a mixture of LiCl-KCl eutectic (electrolyte) and MgO (separator) and NiS_2 (cathode, 0.44 g, 3.6 mmol) were pressed into pellets of diameter 23.6 mm. These pellets were kept under argon before loading into the neutron diffraction sample holder inside the glovebox.

Prior to the *in-situ* neutron diffraction experiment, the battery pellet was loaded into a Swagelok type assembly in an argon-filled glovebox. This enabled electrochemical testing to be carried out

ex-situ at 520 °C in a muffle furnace, using a Maccor battery tester (model 5300). The battery was tested galvanostatically, applying a current density of 22.9 mA cm^{-2}.

Time-of-flight neutron diffraction data were collected on the Polaris diffractometer at the ISIS neutron source, Rutherford Appleton Laboratory, UK. Polaris is a high intensity medium resolution diffractometer and in particular the high intensity lends itself well to fast data collection required during battery discharge. The St Andrews Conductivity Rig, which has been specially developed for the simultaneous collection of neutron diffraction and electrochemical data, which will be described elsewhere, was used for this experiment.[17] The sample holder of the St Andrews Conductivity Rig was adapted for this experiment, by using thin vanadium plate as both current collectors for the electrochemical measurements and for holding the sample in place. Vanadium is an excellent choice in this respect, due to its neutron scattering length of −0.38 fm, meaning that the intensities of the Bragg reflections from the sample holder/current collector are very weak, and make negligible contribution to the diffraction pattern compared to the rest of the battery components. The battery was loaded into the St Andrews Conductivity Rig in the glovebox. All diffraction measurements were carried out under flowing argon due to the air and moisture sensitivity of these samples.

A powder neutron diffraction pattern was collected at room temperature from the undischarged battery (where the molten salt electrolyte would be solid). Following this, the battery pellet was then heated up to 520 °C (at a rate of approximately 4 °C/min) with diffraction data collected in 5 minute steps. After reaching 520 °C, the discharge was started, during which diffraction data were collected isothermally at 520 °C. Good quality diffraction data was collected for 30 minutes at different isopotentials and shorter 5 minute diffraction datasets were collected during discharge and between the isopotentials. During the discharge, electrochemical data were collected potentiostatically using a Kikusui electrochemical interface.

Powder X-ray diffraction data were collected at Diamond Light Source on Beamline I11.[18] Data were collected in Debye Scherrer geometry, using a wavelength of 0.49487 Å at room temperature. The high intensity, Mythen position sensitive detector was used for all data collections. Data were collected on the NiS_2 cathode after the *in-situ* neutron diffraction experiment.

Rietveld refinement was carried out using GSAS.[19] Film plots of diffraction data were created using the WinPlotr function in Fullprof.[20]

Acknowledgements

Conflict of Interest

The authors declare no conflict of interest.

[1] R. A. Guidotti, P. Masset, *J. Power Sources* **2006**, *161*, 1443.
[2] R. A. Guidotti, P. J. Masset, *J. Power Sources* **2008**, *183*, 388.
[3] C. J. Wen, R. A. Huggins, *J. Solid State Chem.* **1981**, *37*, 271.
[4] J. J. M. Griego, M. A. Rodriguez, D. E. Wesolowski, *Adv. X-Ray Anal.* **2013**, *56*, 1.
[5] P. Masset, R. A. Guidotti, *J. Power Sources* **2007**, *164*, 397.
[6] P. J. Masset, R. A. Guidotti, *J. Power Sources* **2008**, *178*, 456.
[7] P. J. Masset, R. A. Guidotti, *J. Power Sources* **2008**, *177*, 595.
[8] G. Kullerud, R. A. Yund, *Journal of Petrology* **1962**, *3*, 126.
[9] R. Y. Lin, D. C. Hu, Y. A. Chang, *Metall. Trans. B* **1978**, *9*, 531.
[10] H. Seim, H. Fjellvag, F. Gronvold, S. Stolen, *J. Solid State Chem.* **1996**, *121*, 400.
[11] M. E. Fleet, *Acta Cryst. B* **1972**, B 28, 1237.
[12] Y. Liu, L. Noren, R. L. Withers, J. Hadermann, G. Van Tendeloo, F. J. Garcia-Garcia, *J. Solid State Chem.* **2003**, *170*, 351.
[13] Y. Yamaguchi, T. Takeuchi, H. Sakaebe, H. Kageyama, H. Senoh, T. Sakai, K. Tatsumi, *J. Electrochem. Soc.* **2010**, *157*, A630.
[14] O. Bergstrom, A. M. Andersson, K. Edstrom, T. Gustafsson, *J. Appl. Crystallogr.* **1998**, *31*, 823.
[15] J. J. Biendicho, M. Roberts, C. Offer, D. Noreus, E. Widenkvist, R. I. Smith, G. Svensson, K. Edstrom, S. T. Norberg, S. G. Eriksson, S. Hull, *J. Power Sources* **2014**, *248*, 900; M. Roberts, J. J. Biendicho, S. Hull, P. Beran, T. Gustafsson, G. Svensson, K. Edstrom, *J. Power Sources* **2013**, *226*, 249; B. Vadlamani, K. An, M. Jagannathan, K. S. R. Chandran, *J. Electrochem. Soc.* **2014**, *161*, A1731.
[16] S. K. Preto, Z. Tomczuk, S. Vonwinbush, M. F. Roche, *J. Electrochem. Soc.* **1983**, *130*, 264.
[17] G. M. Carins, M. O. Jones, R. I. Smith, J. T. S. Irvine, *in preparation* **2016**.
[18] S. P. Thompson, J. E. Parker, J. Potter, T. P. Hill, A. Birt, T. M. Cobb, F. Yuan, C. C. Tang, *Rev. Sci. Instrum.* **2009**, *80*, 075107; S. P. Thompson, J. E. Parker, J. Marchal, J. Potter, A. Birt, F. Yuan, R. D. Fearn, A. R. Lennie, S. R. Street, C. C. Tang, *J. Synchrotron Radiat.* **2011**, *18*, 637.
[19] A. C. Larson, R. B. von Dreele, *Los Alamos National Laboratory Report*, **2004**; B. H. Toby, *J. Appl. Crystallogr.* **2001**, *34*, 210.
[20] T. Roisnel, J. Rodriguez-Carvajal, in *EPDIC 7: European Powder Diffraction, Pts 1 and 2*, Vol. 378–3 (Eds: R. Delhez, E. J. Mittemeijer) **2001**, p. 118; J. Rodriguez-Carvajal, *Physica B* **1993**, *192*, 55.
[21] M. Zeilinger, T. F. Faessler, *Acta Cryst. E* **2013**, *69*, i81; U. Frank, W. Muller, H. Schafer, *Z. Naturforsch. B* **1975**, *B 30*, 10; V. L. Chevrier, J. W. Zwanziger, J. R. Dahn, *J. Alloy. Cmpd.* **2010**, *496*, 25; T. Gruber, S. Bahmann, J. Kortus, *Phys. Rev. B* **2016**, *93*, 144104.
[22] R. D. Shannon, *Acta Cryst. A* **1976**, *32*, 751.
[23] P. Limthongkul, Y. I. Jang, N. J. Dudney, Y. M. Chiang, *J. Power Sources* **2003**, *119*, 604; P. Limthongkul, Y. I. Jang, N. J. Dudney, Y. M. Chiang, *Acta Mater.* **2003**, *51*, 1103.

ARTICLES

Simultaneous collection of powder neutron diffraction data and electrochemical data has been used to determine a new discharge mechanism for a thermal battery utilising NiS_2 as a cathode, which does not involve Ni_7S_6. The evolution of the crystalline phases during battery discharge has been studied and four different nickel-containing phases were observed (NiS_2, NiS, Ni_3S_2 and Ni).

$NiS_2 \longrightarrow NiS \longrightarrow$

$Ni \longleftarrow Ni_3S_2 \longleftarrow$
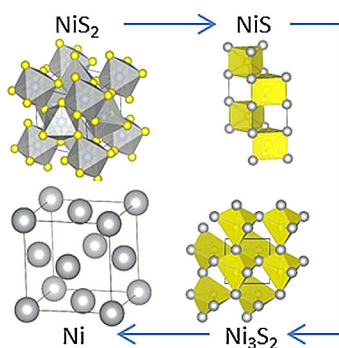
Dr. J. L. Payne*, Dr. J. D. Percival, K. Giagloglou, C. J. Crouch, Dr. G. M. Carins, Dr. R. I. Smith, Dr. R. Comrie, Dr. R. K. B. Gover, Prof. J. T. S. Irvine*

1 – 9

***In-Situ* Thermal Battery Discharge using NiS₂ as a Cathode Material**